<論 文>

東支那海의 潮汐 및 海溢 數値모델*

Mathematical Modelling of Tides and Surges in the East China Sea

崔 秉 昊**
Byung-Ho Choi

要 旨

黃海 및 東支那海와 같은 淺海에서 海流 및 海面變化의 主要因은 潮汐이다. 近年에 垂直積分된 運動方程式 및 連續方程式을 基礎로 한 黃海 및 東支那海의 二次元 水動力學的 數値 모델이 開發되어 潮汐의 主分潮의 振幅, 位相을 滿足스러운 精度로서 再現할 수 있었으며 일련의 數値實驗에 依해 이 海域의 潮汐力學을 理解하는 데 必要한 資料를 提供하였다. 다음 段階로서 黃海 및 東支那海의 三次元 水動力學的 數値모델이 樹立되어 潮流와 定常 均一風에 依한 海流의 垂直分布가 算定되었으며 그 結果가 討議되었다.

ABSTRACT

In semi-enclosed shallow sea areas typified by the Yellow sea and the East China Sea, currents and sea surface variations are predominantly tidal. During the recent years two-dimensional numerical hydrodynamic model of the Yellow Sea and the East China Sea has been developed, based on the vertically-integrated equations of motion and continuity, capable of reproducing amplitudes and phases of the principal components of tides to satisfiable accuracy.

As a subsequent development a three-dimensional hydrodynamical numerical model covering the Yellow Sea and the East China Sea has been formulated to investigate the vertical distribution of horizontal tidal current and the response of the continental shelf sea to steady uniform wind stress field imposed over the surface. Features of the M_2 tidal current and the wind-induced three-dimensional current structure determined from the computation have been examined and discussed.

INTRODUCTION

The tidal phenomena of the Yellow Sea and the East China Sea are extremely complex and studies have been carried out since the beginning of the century. During the late 1920s and early 1930s extensive studies of this area were reported and a considerable number of tidal measurements were made, from which co-tidal (M_2) and co-range (M_2+S_2) charts were prepared (Ogura, 1933).

The numerical methods for solving the partial differential equations which govern tidal motion and meteorological phenomena have been widely used for some years. Based on modelling techniques at the Bidston Observatory, Institute of Oceanographic Sciences, U.K., two numerical models have been established for the study of tidal dynamics of the Yellow Sea and the East China Sea continental shelf sea. One is two-

*第18次 國際測地學 및 地球物理學聯盟總會에서 發表되었음.

**成均館大學 工科大學 土木科 副敎授
Department of Civil Engineering, Sung Kyun Kwan University, Korea

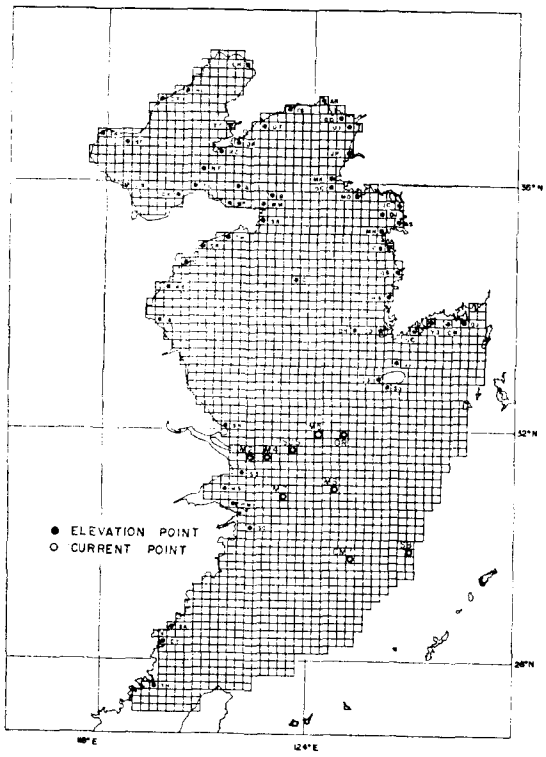

Fig. 1. The Yellow Sea and the East China Sea model finite difference grid.

dimensional in the horizontal based on the vertically integrated equations of motion and continuity and the second model employed is three-dimensional. As shown in Fig. 1. both models extends to the south as far as Northern Taiwan and seaward as far as the edge of the continental shelf edge and have the same grid resolution of 1/5° latitude by 1/4° longitude.

Detailed comparison between the computed results from the model and tidal constants from observation are presented for major constituents of tidal elevation. Recently Larsen and Cannon (1983) utilised the model results of computed current for comparison with a number of current measurement made across the continental shelf along approximately 30°N during the joint USA-China Marine Sedimentation Dynamics Study. They found agreement between the observation and the model thus supporting the assumed boundary conditions and numerical procedure. However they used uppermost current meter data for comparion with depth-averaged current computed from the model.

Subsequently a three-dimensional shelf model was develped to reproduce the tidal current in the region in more detailed manner. As a first step boundary forcing is provided by M_2 tidal elevation only. Reasonable agreement was found between the computed results and observed current from USA-China Marine Sedimentation Dynamics Study. A numerical experiment has been performed with the developed three-dimensional model to determine the response of the shelf sea to stationary wind stress fields suddenly imposed on the shelf for wind directions of NW and SW winds and wind stress of 1.6 dyn/cm². Circulation patterns thereby deduced are briefly discussed.

Times and phases in this study are referenced to 135°E longitude (time zone, -9h).

NUMERICAL MODEL

Two-dimensional Shelf Model

Considering the area covered by the model, the curvature of the earth and the variation with latitude of the Coriolis acceleration are taken into account by adopting spherical co-ordinates. The equations of motion and continuity as used in this model are (Flather 1976, Davies 1976) :

$$\frac{1}{R\cos\phi}\left\{\frac{\partial}{\partial\chi}(Hu)+\frac{\partial}{\partial\phi}(Hv\cos\phi)\right\}+\frac{\partial\xi}{\partial t}=0, \tag{1}$$

$$\frac{\partial u}{\partial t}+\frac{u}{R\cos\phi}\frac{\partial u}{\partial\chi}+\frac{v}{R}\frac{\partial u}{\partial\phi}-\frac{uv\tan\phi}{R}-2\omega\sin\phi v+\frac{k_b u\sqrt{u^2+v^2}}{H}+\frac{g}{R\cos\phi}\frac{\partial\xi}{\partial\chi}=0, \tag{2}$$

$$\frac{\partial v}{\partial t}+\frac{u}{R\cos\phi}\frac{\partial v}{\partial\chi}+\frac{v}{R}\frac{\partial v}{\partial\phi}+\frac{u^2\tan\phi}{R}+2\omega\sin\phi u+\frac{k_b v\sqrt{u^2+v^2}}{H}+\frac{g}{R}\frac{\partial\xi}{\partial\phi}=0, \tag{3}$$

Equations (1) – (3) are vertically integrated hydrodynamical equations where the notation is

t time

χ, ϕ east-longitude and latitude, respectively

ξ	elevation of the sea surface above the undisturbed level
$H=h+\xi$	total depth of water
R	radius of the earth
ω	angular speed of the earth's rotation
k_b	coefficient of bottom friction
g	accelaration due to gravity
u', v'	components of current in directions of χ, ϕ
u, v	respectively at a depth z below the undisturbed sed surface components of depth-mean current given by

$$u=\frac{1}{h+\xi}\int_{-h}^{\xi} u'(z)\,dz,\ v=\frac{1}{h+\xi}\int_{-h}^{\xi} v'(z)\,dz$$

These equations, formulated with a quadratic law of bottom friction, are integrated on a staggered finite difference grid using the scheme described by Roberts and Weiss (1967) which centres the advective terms in time and space. The method employed for implementing this scheme is described by Flather and Heaps (1975) and Flather (1976).

Initial and boundary conditions required for the solution of equations (1) to (3) are as follows:

At $t=0$: $u(\chi, \phi, t)$, $v(\chi, \phi, t)$ and $\xi(\chi, \phi, t)$

are specified for all positions at which the equations are to be solve. At a land boundary: the component of the flow normal to the boundary is permanently zero:

$u\cos\theta+v\sin\theta=0$

Where θ is the angle between the normal to the coast directed out of the sea region and the χ axis. Therefore

$u=0$ is the boundary condition at a ϕ -directed land boundary

$v=0$ is the boundary condition at a χ -directed land boundary.

Along an open boundary, elevation is specified as a function of time and position along the boundary: $\xi(\chi, \phi, t)$ is supplied.

In shallow sea areas provision is made in the numerical scheme for representing the drying of tidal flats.

In the model, tidal constants of M_2, S_2, K_1 and O_1 tides deduced from the shelf edge of existing charts and a limited number of analyses of coastal and island tidal records are introduced for specifying the open boundary condition of the model. A uniform value of 0.0025 was used for a coefficient of bottom friction. To satisfy explicit stability condition the time-step chosen was four lunar minutes. The computation of ξ, u, v generated from the initial state of rest, $\xi=u=v=0$ at $t=0$ specifying the composite M_2, S_2, K_1 and O_1 tidal elevation along the open boundaries while zero normal velocities is specified at land boundaries. The model was run for 17 days.

Harmonic analyses for each of the model elements were performed over 15 days of hourly data after discarding the first two days of data. Subsequently computed tidal charts are presented and comparison between the computed and observed distribution of the M_2, S_2, K_1, O_1 tides are made.

Three-dimensional Shelf Model

The equations of continuity and motion for homogenous water neglecting non-linear terms, shear in the horizontal and the direct influence of the tide-generating potentials, may be written in spherical polar coordinates as (Davies, 1980) :

$$\frac{\partial\xi}{\partial t}+\frac{1}{R\cos\phi}\left(\frac{\partial}{\partial\chi}\int_0^h u\,dz+\frac{\partial}{\partial\phi}\int_0^h v\cos\phi\,dz\right)=0, \tag{4}$$

$$\frac{\partial u}{\partial t}-\gamma v=\frac{-g}{R\cos\phi}\frac{\partial\xi}{\partial\chi}+\frac{\partial}{\partial z}\left(N\frac{\partial u}{\partial z}\right), \tag{5}$$

$$\frac{\partial v}{\partial t}+\gamma u=\frac{-g}{R}\frac{\partial \xi}{\partial \phi}+\frac{\partial}{\partial z}\left(N\frac{\partial v}{\partial z}\right), \tag{6}$$

where γ Coriolis parameter ($\gamma=2\omega\sin\phi$)

ρ the density of sea water

N coefficient of vertical eddy viscosity

In order to solve (4), (5) and (6) for ξ, u and v, the appropriate boundary conditions at sea surface and sea bed have to be specified. For tides, the surface condition is

$$-\rho\left(N\frac{\partial u}{\partial z}\right)_0=-\rho\left(N\frac{\partial v}{\partial z}\right)_0=0, \tag{7a, b}$$

with the suffix zero denoting evaluation at $z=0.$, For surges

$$-\rho\left(N\frac{\partial u}{\partial z}\right)_0=F_s,\quad -\rho\left(N\frac{\partial v}{\partial z}\right)_0=G_s \tag{8a, b}$$

where Fs, Gs, denote the component of surface wind stress in the χ and ϕ directions. Assuming a slip boundary condition at the sea bed ($z=h$) and using a quadratic law of bottom friction yields:

$$-\rho\left(N\frac{\partial u}{\partial z}\right)_h=k_b\rho u_h\ (u_h^2+v_h^2)^{1/2} \tag{9a}$$

$$-\rho\left(N\frac{\partial v}{\partial z}\right)_h=k_b\rho v_h\ (u_h^2+v_h^2)^{1/2} \tag{9b}$$

where k_b is the coefficient of quadratic bottom friction, taken as constant.

Expanding the two components of velocity u, v in terms of m depth-dependent function $f_r(z)$ (the basis functions) and the horizontal space and time dependent coefficient $A_r(\chi,\phi,t)$ and $B_r\ (\chi,\phi,t)$ gives:

$$u(\chi,\phi,z,t)=\sum_{r=1}^{m}A_r(\chi,\phi,t)\ f_r(z), \tag{10}$$

$$v(\chi,\phi,z,t)=\sum_{r=1}^{m}B_r(\chi,\phi,t)\ f_r(z), \tag{11}$$

Using the Galerkin method in the vertical space domain, Eqs (5) and (6) are multiplied by each basis functions f_k and integrated over the region 0 to h with respect to z. By integrating the term involving the vertical eddy viscosity, boundary conditions (7a, b) (8a, b) and (9a, b) can be incorporated, giving

$$\int_0^h\frac{\partial u}{\partial t}\ f_k dz=\gamma\int_0^h vf_k dz-\frac{g}{R\cos\phi}\frac{\partial\xi}{\partial\chi}\int_0^h f_k dz-f_k(h)\,k_b u_h\ (u_h^2+v_h^2)^{1/2}$$
$$-\int_0^h N\frac{\partial u}{\partial z}\frac{\partial f_k}{\partial z}\,dz, \tag{12}$$

$$\int_0^h\frac{\partial v}{\partial t}\ f_k dz=-\gamma\int_0^h uf_k dz-\frac{g}{R}\frac{\partial\xi}{\partial\phi}\int_0^h f_k dz-f_k(h)\,k_b v_h(u_h^2+v_h^2)^{1/2}$$
$$-\int_0^h N\frac{\partial v}{\partial z}\frac{\partial f_k}{\partial z}\,dz, \tag{13}$$

where $k=1, 2, \cdots, m$. From Eqs (12) and (13) the bottom boundary conditions occur in these equations as products with $f_k(h)$ and therefore if this product is to be nonzero, the f_k must be chosen such that

$$f_k(h)\neq 0 \tag{14}$$

for $k=1, 2, \cdots\cdots, m$.

For the choice of basis functions $f_r(z)$ Davies (1980) has shown that an expansion of only 10 cosine functions is sufficient to accurately reproduce the depth variation of current and has applied such an expansion to the computation of the tide and wind-induced circulation of the North-West European Continental Shelf.

In the present study adopting the expansion of 10 cosine functions
with f_r given by

$$f_r=\cos\alpha_r\frac{z}{h} \tag{15}$$

and suitable choice for α_r is

$$\alpha_r=(r-1)\pi,\quad r=1,2,\cdots,m. \tag{16}$$

in which case

$$f_r'(0)=0, \tag{17}$$

and

$$f_r'(h)=0, \tag{18}$$

where $f_r'=df_r/dz$.

The particular case in which the vertical eddy viscosity N is independent of depth coordinate Z is considered, the f_r given by Eq (15) are eigen-functions of

$$\frac{d}{dz}\{N(\chi,\phi,t)\ f_r'(z)\}=-\lambda_r(\chi,\phi,t)f_r(z) \tag{19}$$

with eigenvalues $\lambda_r(\chi,\phi,t)$ given by

$$\lambda_r(\chi,\phi,t)=N(\chi,\phi,t)\alpha_r^2/h^2 \tag{20}$$

Integrating by parts the terms involving N in (12) and (13) using (19), (20), (17), and (18) and substituting expansions (10) and (11) into (12), and (13) gives a'set of partial differential equations involving ξ and A_r and B_r. Details of formulation was given by Davies (1980) and will not restated here.

These equations can then be integrated forward through time to find the variation of ξ, A_r, B_r over the modelled sea area subject to initial and boundary conditions. Currents at any depth can be calculated from the A_r and B_r using expansion (10) and (11). In order to solve the equations it is necessary to discretize in the horizontal and with time. Discretization in the horizontal is accomplished using a staggered finite-difference grid, in which ξ, u, v are evaluated at different grid points. Solutions are generated from a state of rest, expressed by

$$\xi=A_r=B_r=0 \text{ at } t=0,\quad (r=1,2,\cdots\cdots,m). \tag{21}$$

Along a closed boundary the normal component of current is set to zero, for all $t\geq 0$, thus

$$A_r\cos\theta+B_r\sin\theta=0,\quad (r=1,2,\cdots\cdots,m). \tag{22}$$

where θ denotes the inclination of the normal to the direction of increasing χ.

Along the open bounaries of the model, M_2 tidal input determined from the two-dimensional model (Choi, 1980) is specified and radiation condition is employed to allow disturbances from the interior of the model to pass outward. This condition involves a prescribed relation between the total normal component of depth-mean current q and total elevation ξ given by:

$$q=q_T+\frac{c}{h}(\xi-\xi_T) \tag{23}$$

where $c=(gh)^{1/2}$, ξ_T-the change in sea surface elevation arising from the M_2 tide is given by:

$$\xi_T=H_{M_2}\cos\{\sigma_{M_2}-k_{M_2}\} \tag{24}$$

and

$$q_T=Q_{M_2}\cos\{\sigma_{M_2}t-\gamma_{M_2}\} \tag{25}$$

In Eqs (24) and (25) H_{M_2} and Q_{M_2} denote amplitute of M_2 tidal elevation and the amplitude of the normal component of depth-mean M_2 tidal current. Also k_{M_2} and γ_{M_2} denote the phase of the M_2 tidal elevation and the phase of the normal component of depth-mean M_2 tidal current. These values were derived previously in computing the distribution of the M_2 tide on the East China Sea continental shelf with a two-dimensional model. Using Eq (23) with ξ_T and q_T determined from (24), and (25), the depth-mean current around the edge of the continental shelf may be computed.

However Eq (23) gives no information on the contribution of the various terms in the expansion to the depth-mean current, it is necessary to make an assumption about the contribution of each term in expansions (10) and (11) to this depth-mean current. The assumption made was that only the first term in each expansion contributed to the current at the continental shelf edge.

$$A_r=B_r=0,\quad (r=2,3,\cdots\cdots,m), \tag{26}$$

and A_1 and B_1 are given by

$$A_1=\frac{q_u}{a_1},\quad B_1=\frac{q_v}{a_1}\left(a_1=\frac{1}{h}\int_0^h f_1(z)\,dz\right)$$

where q_u and q_v are respectively the u and v components of depth-mean current given by (23). Heaps (1972) has shown that above assumption does not severely affect the computed current profiles within the theree-dimensional region.

COMPARISON BETWEEN OBSERVED AND COMPUTED TIDES

Tidal Elevation from 2D Model

The model results are presented by comparing the observed harmonic constants for various locations (nearby station from the elevation point marked as •) shown in Fig. 1 with those computed from the Model. Table 1 shows the comparison of the observed and calculated amplitudes and phases of M_2, S_2, K_1 and O_1 tides for these sites. Fig. 2-Fig. 5 show calculated amplitudes and phases of these constituents, plotted against observed values. Errors are about 10% in amplitude and 10 degrees in phase for the semi-diurnal tides (M_2, S_2). For diurnal tides (K_1, O_1), there is less accuracy in amplitude while the agreement between the observed and calculated phases is reasonable.

Table 1. Comparison of observed and calculated amplitude H(m) and phase k(degree referred to 135°E) for the M_2, S_2, K_1, O_1 tides.

Station	Code	Position of Station	M_2 (obs)		M_2 (cal)		S_2 (obs)		S_2 (cal)		O_1 (obs)		O_1 (cal)		K_1 (obs)		K_1 (cal)	
			H	K	H	K	H	K	H	K	H	K	H	K	H	K	H	K
Lia Ho	LH	40°38′N 122°10′E	1.17	179	0.92	187	0.33	234	0.24	256	0.26	79	0.29	94	0.33	116	0.38	125
Chinwangtao	CT	39°54′N 119°37′E	0.14	346	0.34	43	0.05	57	0.11	110	0.21	82	0.17	94	0.27	116	0.23	123
Taku	TK	38°59′N 117°42′E	0.94	130	0.67	141	0.24	199	0.20	209	0.18	133	0.17	134	0.25	163	0.21	167
Tyoto	TT	39°18′N 121°40′E	0.65	62	0.65	50	0.22	113	0.20	114	0.20	50	0.20	50	0.27	81	0.27	77
Ryozun	RZ	38°48′N 121°15′E	0.84	337	0.69	332	0.26	25	0.20	29	0.17	359	0.17	352	0.23	28	0.24	16
Nanfanchen	NF	38°21′N 120°54′E	0.60	337	0.49	337	0.17	35	0.15	37	0.04	35	0.07	29	0.06	28	0.09	24
Tangluantsu	TL	37°59′N 120°41′E	0.56	321	0.40	328	0.10	30	0.12	31	0.07	166	0.03	159	0.09	252	0.03	226
Hainlutu	HL	40°08′N 120°12′E	0.13	237	0.13	185	0.02	286	0.05	245	0.26	89	0.24	90	0.37	136	0.26	120
Sha-lei-tein tao	ST	38°56′N 118°31′E	0.60	96	0.46	115	0.20	165	0.13	181	0.26	121	0.15	121	0.20	155	0.19	155
Li Tsin Ho Bar	LB	37°53′N 118°40′E	0.40	208	0.31	207	0.10	277	0.06	240	0.10	146	0.13	141	0.20	180	0.17	176
Chimutao Kaochiao	CK	37°41′N 120°13′E	0.50	318	0.24	313	0.10	28	0.07	23	0.10	183	0.09	164	0.20	225	0.10	204
White Rock Point	WP	37°29′N 121°38′E	0.60	340	0.61	331	0.20	31	0.19	28	0.10	273	0.10	300	0.20	340	0.16	330
Dairen	DR	38°56′N 121°39′E	0.99	327	0.91	318	0.29	15	0.25	29	0.20	342	0.22	352	0.27	13	0.31	2
Dai Tyozando	DT	39°16′N 122°55′E	1.32	305	1.22	297	0.42	351	0.38	351	0.25	328	0.26	328	0.33	356	0.37	355
Takushan	TS	39°46′N 123°33′N	1.93	295	1.43	288	0.42	327	0.44	341	0.24	304	0.29	323	0.37	350	0.41	348
Amnok R.	AR	40°07′N 124°24′E	0.87	1	0.90	3	0.25	50	0.24	55	0.26	343	0.29	2	0.27	3	0.36	33
Off Chefoo	A	37°57′N 121°55′E	0.74	332	0.54	323	0.22	32	0.16	22	0.13	294	0.12	316	0.18	338	0.18	343
Off Shantung	B	37°37′N 122°47′E	0.20	315	0.21	305	0.06	15	0.05	1	0.16	289	0.16	305	0.23	333	0.23	333
Weiheiwei	WW	37°30′N 122°10′E	0.59	341	0.52	336	0.18	26	0.15	36	0.13	280	0.12	303	0.22	323	0.19	333
Chintau	CU	36°05′N 120°19′E	1.25	174	0.97	165	0.39	213	0.31	213	0.21	318	0.18	322	0.27	10	0.21	2
Central Yellow Sea	C	35°39′N 123°45′E	0.83	86	0.71	89	0.29	126	0.22	138	0.10	274	0.13	275	0.14	313	0.16	298
Side Saddle	SS	30°40′N 122°38′E	1.20	324	1.56	358	0.53	1	0.68	11	0.17	174	0.18	198	0.27	208	0.25	225
Gade	GD	39°31′N 124°40′E	2.08	276	1.96	291	0.68	322	0.52	358	0.27	313	0.30	327	0.42	345	0.42	352
Unmu I.	UI	29°25′N 125°07′E	2.22	337	2.06	302	0.76	220	0.58	348	0.30	315	0.31	323	0.48	352	0.43	348
Jinnampo	JP	38°38′N 125°00′E	1.56	250	1.60	248	0.60	306	0.49	301	0.25	309	0.29	305	0.37	344	0.42	323
Mengkeumpo	MK	38°11′N 124°47′E	1.12	222	1.03	220	0.38	265	0.33	255	0.24	277	0.25	294	0.34	325	0.35	318
Daechungdo	DC	37°50′N 124°43′E	0.99	178	0.94	173	0.42	226	0.32	237	0.27	283	0.25	290	0.31	310	0.34	314
Moodo	MD	37°44′N 125°33′E	1.98	158	1.90	161	0.74	202	0.65	215	0.31	281	0.28	281	0.34	314	0.36	303
Inchon	IC	37°29′N 126°37′E	2.92	148	2.74	161	1.13	198	0.96	221	0.26	276	0.30	283	0.39	306	0.37	305
Duckjuckdo	DJ	37°15′N 126°09′E	2.48	139	2.30	152	0.90	192	0.87	209	0.30	274	0.29	278	0.40	297	0.37	300
Asan	AS	36°58′N 126°47′E	3.03	144	2.72	157	1.08	196	0.95	217	0.28	264	0.28	282	0.40	305	0.37	304
Mohangri	MH	36°47′N 126°08′E	2.20	122	2.09	129	0.78	168	0.73	184	0.28	264	0.28	267	0.37	294	0.36	288
Chonsu Bay	CB	36°23′N 126°26′E	2.26	115	2.06	109	0.84	162	0.72	162	0.27	259	0.28	258	0.39	286	0.35	278
Gunsan	GS	35°59′N 126°43′E	2.13	109	2.15	98	0.74	157	0.74	152	0.25	254	0.27	253	0.31	287	0.35	273
Hampeong Bay	HB	35°09′N 126°05′E	1.87	75	1.73	74	0.61	116	0.59	125	0.27	238	0.26	241	0.40	263	0.33	260
Chindo	CD	34°30′N 126°12′E	1.13	49	1.20	23	0.41	61	0.42	66	0.23	219	0.24	215	0.30	247	0.31	232
Daeheuksando	DH	34°41′N 125°26′E	1.02	48	0.98	28	0.35	85	0.31	72	0.18	233	0.19	221	0.24	253	0.26	240
Sangkau Bay	SB	37°03′N 122°29′E	0.70	72	0.71	86	0.10	132	0.16	143	0.20	281	0.16	296	0.30	341	0.21	329
Tau Tsui Head	TH	36°44′N 121°39′E	1.00	117	0.94	121	0.20	164	0.29	170	0.20	306	0.17	305	0.30	0	0.20	340
Star Reef	SR	36°23′N 120°50′E	1.20	150	0.99	140	0.30	193	0.32	189	0.20	318	0.17	313	0.30	11	0.20	350
Wang Chia Tai Bay	WB	35°32′N 119°45′E	1.20	183	1.18	199	0.40	216	0.34	250	0.20	338	0.19	337	0.30	25	0.22	13
Bamboo I.	BI	34°45′N 119°26′E	1.20	216	1.24	221	0.40	251	0.40	279	0.20	357	0.20	349	0.30	45	0.24	25
Sang Chia Chun	SN	32°01′N 121°42′E	1.10	4	1.24	46	0.40	50	0.53	100	0.20	139	0.10	162	0.20	191	0.15	197
Middle Seshan	MS	30°36′N 121°38′E	1.50	22	1.41	28	0.60	60	0.52	118	0.20	203	0.19	224	0.50	228	0.25	253
Hai-Ho Men	HM	30°06′N 121°54′E	1.10	336	1.06	339	0.40	10	0.42	84	0.20	190	0.19	215	0.30	226	0.26	241
Shin Phu Road	SD	29°12′N 122°01′E	1.50	290	1.65	314	0.60	328	0.65	11	0.23	207	0.20	198	0.30	238	0.24	229
San-tu Ao	SA	26°38′N 119°42′E	2.57	339	1.98	332	0.79	17	0.60	23	0.24	225	0.26	216	0.35	261	0.30	247
Ching Yu	CY	26°08′N 119°38′E	2.04	350	1.98	342	0.58	28	0.57	28	0.23	241	0.26	219	0.25	269	0.29	250
Tate Hsii	TH	25°05′N 119°03′E	2.00	5	2.04	15	0.60	47	0.33	51	0.20	251	0.23	231	0.30	261	0.29	266
Chaguido	CG	33°18′N 126°09′E	0.76	322	0.89	324	0.29	333	0.34	10	0.16	198	0.22	199	0.25	223	0.30	218
Seoguipo	SG	33°14′N 126°33′E	0.77	288	0.94	293	0.34	318	0.38	341	0.18	188	0.23	187	0.24	209	0.30	208
Jeju	JJ	33°31′N 126°35′E	0.66	318	0.85	314	0.30	343	0.31	349	0.17	198	0.19	192	0.23	220	0.27	213
Gegeum Channel	GC	34°30′N 127°09′E	1.10	291	1.17	283	0.53	314	0.49	317	0.18	178	0.18	161	0.30	197	0.28	184
Yeosu	YS	34°44′N 127°45′E	1.02	267	1.11	270	0.47	293	0.46	304	0.13	157	0.15	156	0.21	185	0.23	179
Geojedo	GJ	34°43′N 128°36′E	0.75	258	0.82	258	0.29	281	0.34	293	0.06	137	0.09	156	0.09	161	0.15	174
Choongmoo	CM	34°51′N 128°25′E	0.80	265	1.00	264	0.37	296	0.41	298	0.12	166	0.13	157	0.16	181	0.20	177

The general tidal behaviour in the system may be conveniently presented by co-tidal lines and co-amplitude lines. Fig 6-Fig 9 show model computed M_2, S_2, K_1 and O_1 tidal charts. The predominant feature is amphidromic regions located in the Gulfs of Pohai and Liautung, off-Shantung Promontory and offshore region in the east coast of China. The existence of these amphidromic points may be explained by the ratio of the fundamental period of the system 46h, which is calculated by simple analytic model (Defant, 1960) to that of tide generating force about 3.7 for the semi-diurnal tides and about 1.9 for the diurnal tides, thus having four amphidromes in the semi-diurnal tidal charts and two amphidromes in the diurnal charts.

There is a good qualitative agreement between the model computed charts and existing charts (Ogura, 1933) although there is some deterioration in areas where the bottom togography is known to be complex and uncertain, particularly mid-Chinese coast where there is a large number of sand bars unresolved by the model, and in the region of amphidromic points in the Gulf of Liautung where tidal constants change substantially over a mesh element. From the charts, it is seen that both diurnal and semi-diurnal tides at the shelf edge propagate in a northwesterly direction to the entrance of the Yellow Sea (from Shanghai to the southern tip of Korea) as progressive waves. A part of tides entering across the shelf rotates counter-clockwise with its center at northern end of Taiwan (degenerate amphidromic points shown in M_2 tidal chart), counter-clockwise to southwest and progress to Taiwan Strait. On entering the Yellow Sea, the tides progress to north along the west coast of Korea and after reaching the north shore of Yellow Sea, the tide turns its direction to west and progress to Strait of Pohai. Then the tide progresses in a counter clockwise direction along the coast in the Gulfs of Liautung and Pohai and progresses to east along the south shore of the Pohai making a complete revolution within Gulfs of Liautung and Pohai. The tides, after coming out from Pohai, progress down first to the southwest and then southeast along the coast of China.

Some features of the model results are as follows:

Semi-diurnal tides (See Fig. 6. and Fig. 7)

1) Maximum amplitudes of the M_2, S_2, elevations are found at Inchon and Asan in Kyonggi Bay,
2) Both M_2, S_2 tides progress very slowly in the southwest corner of Korea, and near the Changsan Promontory (38°N) off the west coast of Korea.
3) A speculated position of amphidromic point in the southeast off Shantung Promontory by Ogura at about latitude 35°N, longitude 121.5°E agrees well with the model results,

Diurnal tides (See Fig. 8 and Fig. 9)

1) Maximum amplitudes of the K_1, O_1 elevations are found at Unmu Island in Seohan Bay,
2) Amplitudes of diurnal tides do not increase as much as those of semi-diurnal tides in Kyonggi Bay, which may be partly due to the difference in the direction of propagation of tides, the diurnal waves approaching the coast more obliquely,
3) The pattern of progress of diurnal tides in the Yellow Sea is similar to semi-diurnal tides but the change in velocity of the diurnal tides is greater over the shelf edge to entrance of the Yellow Sea and along the west coast of Korea.

Tidal Current from 2D Model

Fig. 10-Fig. 13 show the calculated M_2, S_2, K_1 and O_1 tidal ellipses of selected points in the Yellow Sea and the East China Sea. The ellipses chart give the magnitude and the direction of propagation of the tidal currents representing maximum and minimum velocity as major and minor axes respectively and sense of rotation from 0 lunar hour (referenced to 135°E) is also indicated by arrows.

Some of the model results are as follows:

1) The velocity of semi-diurnal currents is high at Jeju Strait (between southwest corner of Korea and

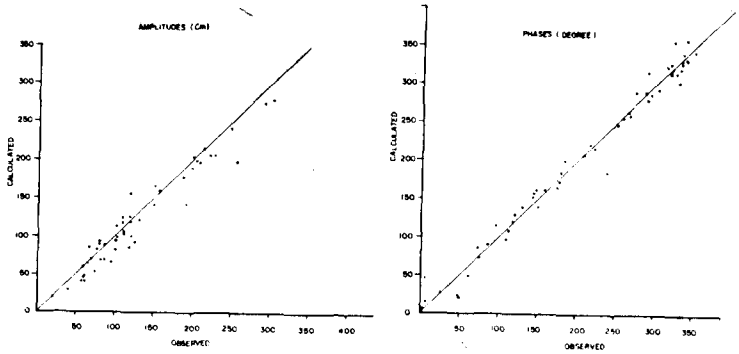

Fig. 2. Comparison between calculated and ovserved amplitudes and phases of the M_2 tide.

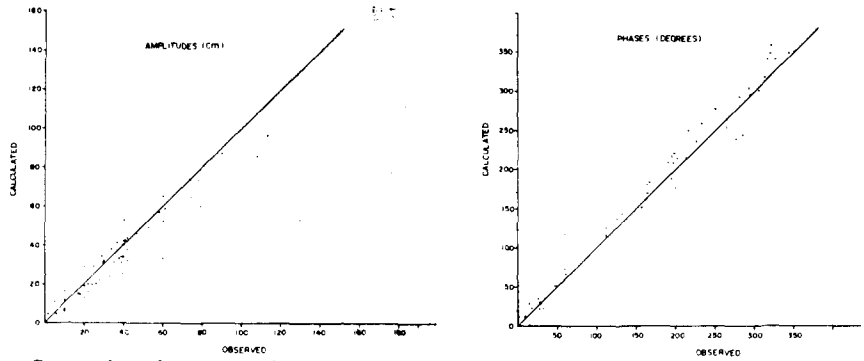

Fig. 3. Comparison between calculated and ovserved amplitudes and phases of the S_2 tide.

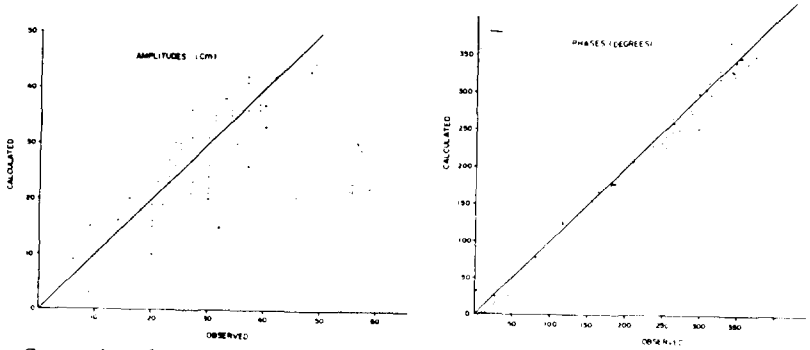

Fig. 4. Comparison between calculated and observed amplitudes and phases of the K_1 tide.

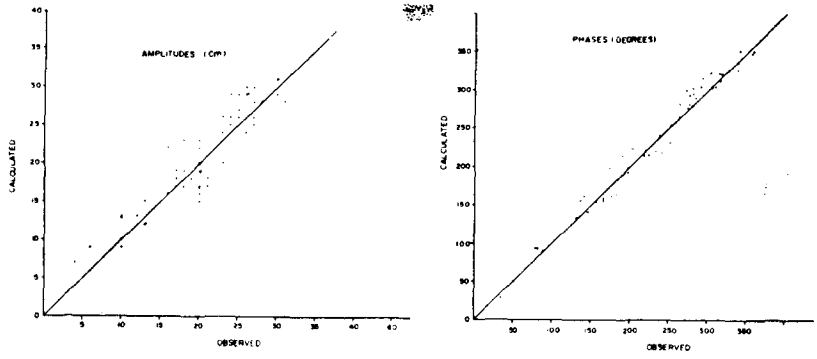

Fig. 5. Comparison between calculated and observed amplitudes and phases of the O_1 tide.

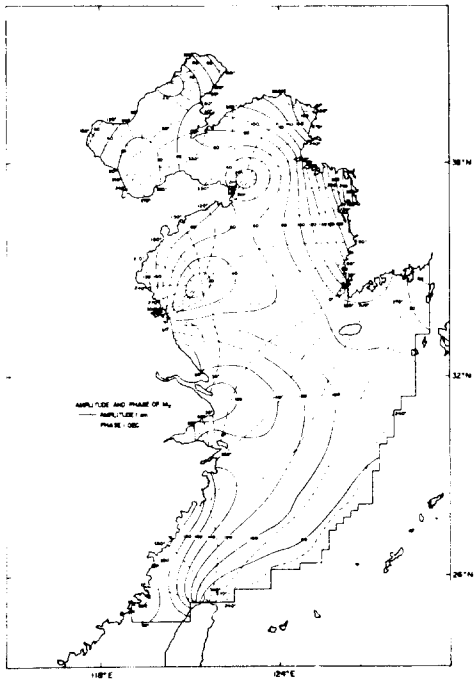

Fig. 6. Computed M_2 tidal chart.

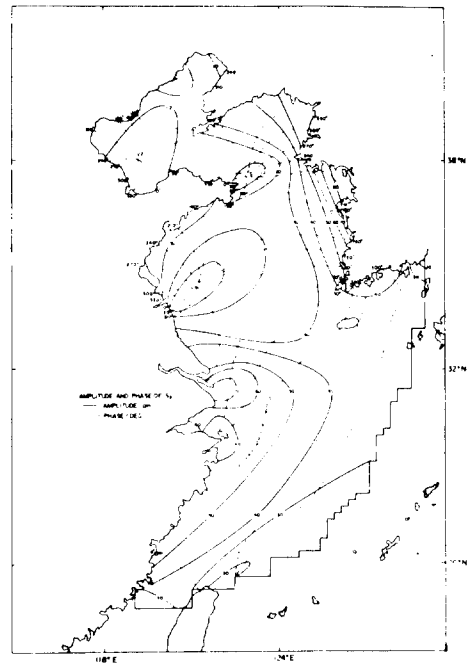

Fig. 7. Computed S_2 tidal chart.

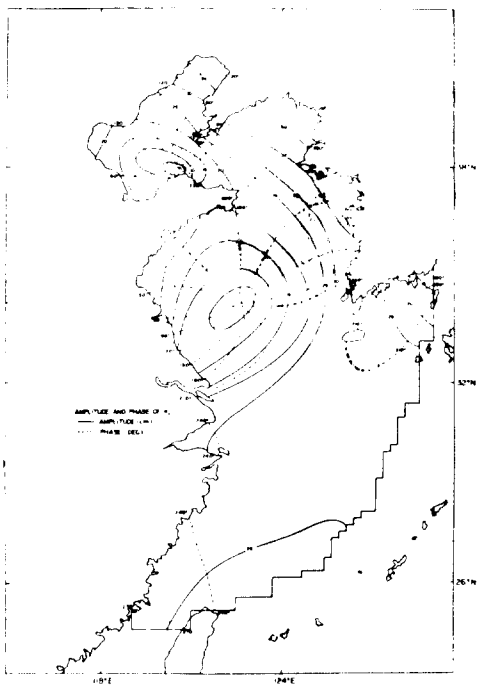

Fig. 8. Computed K_1 tidal chart.

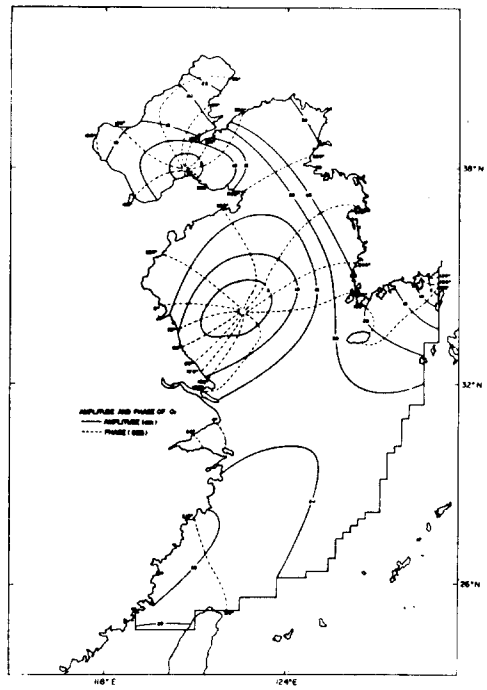

Fig. 9. Computed O_1 tidal chart.

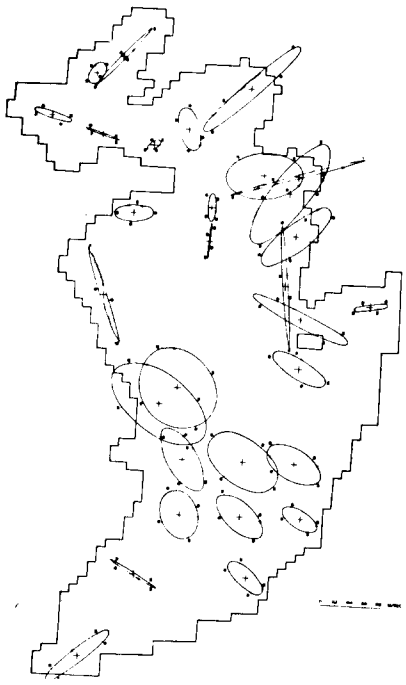

Fig. 10. Calculated M_2 tidal current ellipses

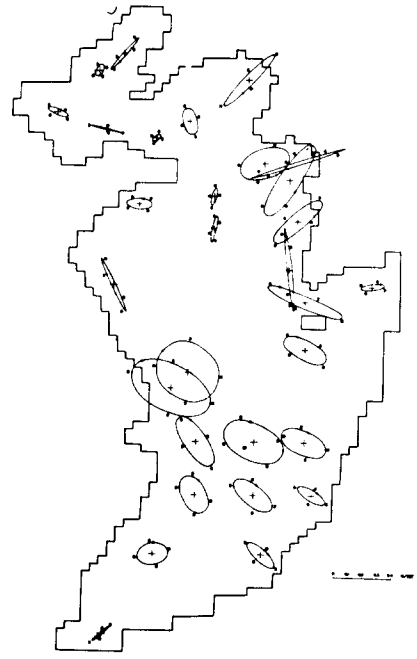

Fig. 11. Calculated S_2 tidal current ellipses

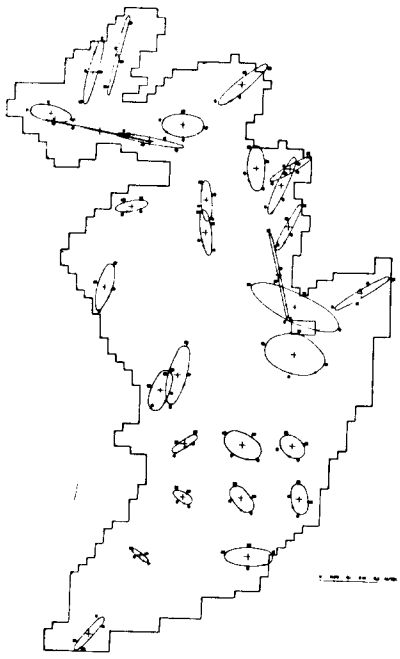

Fig. 12. Calculated K_1 tidal current ellipses

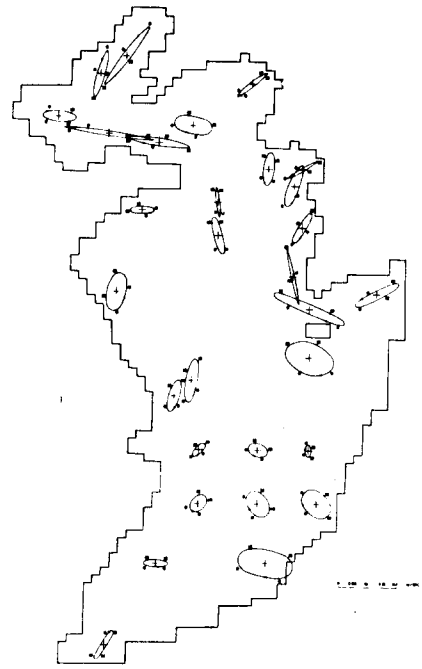

Fig. 13. Calculated O_1 tidal current ellipses

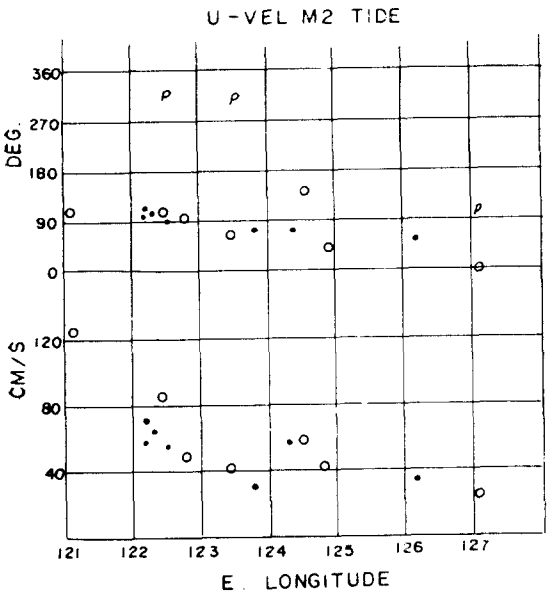

Fig. 14. The distribution in amplitude and phase of the U component of velocity for the M_2 tide.

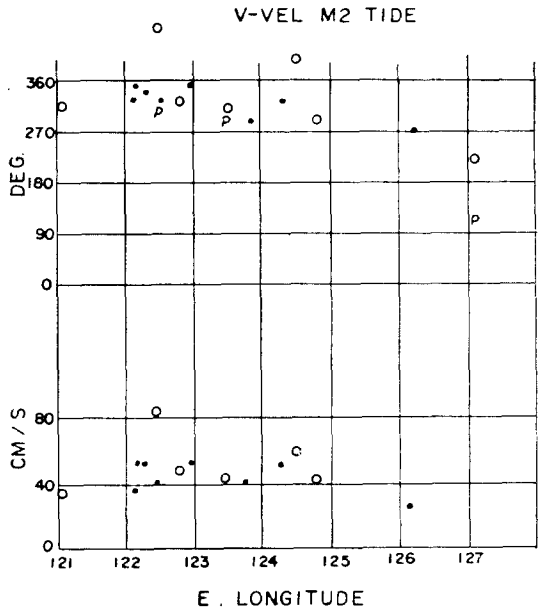

Fig. 15. The distribution in amplitude and phase of the V component of velocity for M_2 tide.

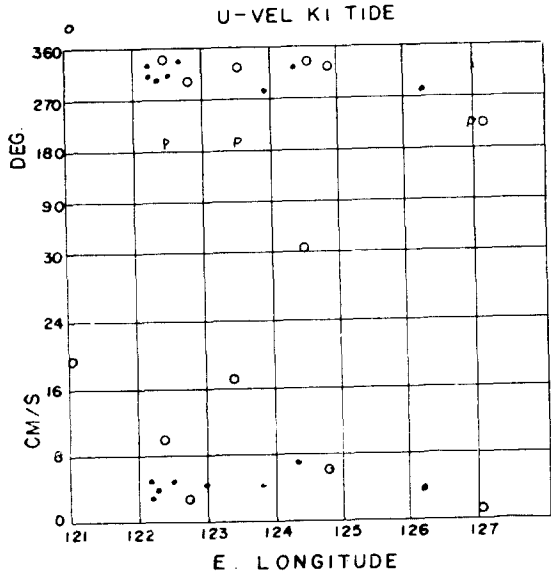

Fig. 16. The distribution in amplitude and phase of the U component of velocity for the K_1 tide.

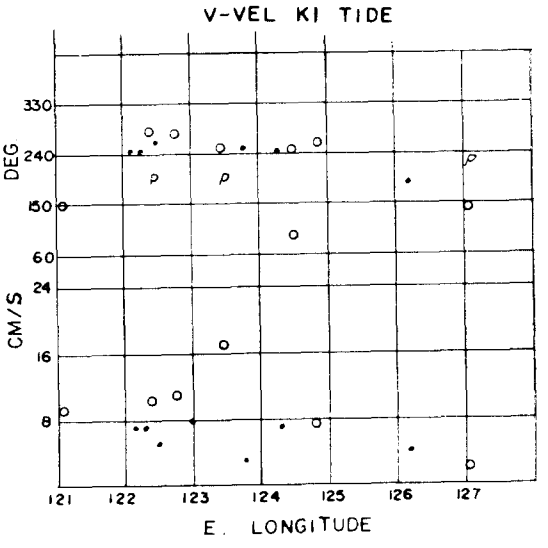

Fig. 17. The distribution in amplitude and phase of the V component of velocity for the K_1 tide.

Jeju Island) and also along the west coast of Korea (southwest corner of Korea, Kyonggi Bay, Seohan Bay) and at the entrance to the Yangtse River and is of the order of 100cm/sec,

2) The weakest semi-diurnal currents are to be found along the south coast of the Gulf of Pohai and are of the order of 20cm/sec,
3) The regions of strong diurnal currents are similar to those of semi-diurnal currents where they are of the order of 40cm/sec; other stronger diurnal currents computed are found to be at the narrows of the Kyushu Islands where they are of the order of 70cm/sec and at Pohai Strait and Gulf of Liautung where they are about 40cm/sec,
4) Generally speaking, tidal currents over the shelf from the continental edge to the entrance of the Yellow Sea are rotatory, in a clockwise direction through their periods, while the currents in the Yellow Sea are rectilinear following their direction of propagation along the coast.

Larsen and Cannon (1983) recently reported a number of current observations made across the continental shelf along approximately 30°N. They found general agreement between the observations and model computation as illustrated in Figs. 14-17. Fig. 14 compares the U component of velocity for the M_2 tide, Fig. 15 the V component of velocity for the M_2 tide. Fig. 16 and Fig. 17 compare the velocity components associated with the K_1 constituent. In the figures phases of tidal elevations are indicated by P. The dots are computed model results, the open circles are the observations collected during the USA-China Marine Sedimentation Dynamics Study Program. In the comparison, only data from the uppermost current meter at each station were shown in the figures. They also found general agreement between orientation of the ellipses from the observations and the model.

Tidal Current from 3D Model

The 3D model results for current computations are presented by comparing the observations (nearby current rigs from the point marked as 0) shown in Fig. 1. with those computed from the model.

In order to make the comparison between computed and observed currents it is necessary to compare amplitudes and phases of the U component and V component of current. Computed and observed values of amplitude H (Cm S^{-1}) and phase K (degree referred to 135°E) for U and V at nine current meter rigs are given in Table 2. It is seen from the table that general agreement between the observations and the model results have been demonstrated. It is worth mentioning that positional discrepancy between the current observation points and nearby model calculation points could be in error by as much as 0.2 degrees. Initial calculations were made at three representative depths in the present study although the model could compute a continuous current profile with depth. The amplitude of M_2 tidal current was computed to within 15% at 55% of the current meter rigs and its phase to within 10° at 80% of the rigs.

CURRENT DRIVEN BY STEADY UNIFORM WIND STRESS

A uniform steady wind was blown for 36 hours from the state of rest. Northwesterly and southwesterly wind directions and wind stress of 1.6 dyn/cm^2 was chosen to investigate the response of shelf sea to these stationary wind stress fields suddenly imposed on the sea surface area. The spatial distribution of vectors of wind-induced current at three representative depth is illustrated in Fig. 18 for northwesterly wind stress field and in Fig. 19 for southwesterly wind stress field.

As shown surface currents are directly responded to the direction of wind stress imposed. Under northwesterly wind, it was shown that clockwise gyres at the mid-depth are formed in the region of Liautung Gulf, northern part of Pohai Bay, Seohan Bay, outer Kyonggi Bay and southern part of Shantung Peninsula.

Table 2. Comparison of observed and computed amplitude (Cm S^{-1}) and phase K (degree referred to 135°E) for U and V component of M_2 tidal current.

Current meter rig	Position (Latitude / Longitude)	Observed U H	Observed U K	Observed V H	Observed V K	depth	Calculated U H	Calculated U K	Calculated V H	Calculated V K	depth
M2	31.40N 122.37E	84	129	83	124	4	77	116	63	71	Surface
M4	31.25N 122.82E	47	117	48	349	2	62	110	51	355	Surface
		30	98	34	325	44	32	105	25	348	bottom
M5	32.00N 124.50E	47	78	51	342	20	59	92	54	354	mid-depth
M7	30.33N 123.44E	40	86	43	335	5	37	95	45	323	surface
		20	94	27	334	60	21	92	24	310	bottom
SB	28.91N 127.25E	27	6	17	241	177	18	12	12	240	bottom
MS	30.52N 124.80E	42	54	41	316	23	48	61	39	314	mid-depth
		32	42	30	302	45	29	56	22	308	bottom
SDS	31.16N 122.46E	12	78	23	321	bottom	28	111	24	359	bottom
CM7	28.65N 125.45E	31	21	23	259	20	31	23	26	260	mid-depth
OR	32.00N 125.15E	45	86	57	348	23	57	84	49	342	mid-depth

A bottom return current along the thalweg of the Yellow Sea and the East China Sea continental shelf could be identified and bottom flows are discharged through the Taiwan Strait.

Under southwesterly wind it is shown that counter-clockwise gyres at the mid-depth are formed in the region of northern part of Shantung peninsula, Seohan Bay, outer Kyonggi Bay. A bottom return current along the thalweg of the Yellow Sea also could be identified and part of these flows are discharged through the Jeju Strait. The magnitude of horizontal current is diminished vertically down to the sea bed, however relatively strong bottom current occur along the Chinese coast and the west coast of Korea. From the experiments, it is seen that there are significant variation in both magnitude and direction of horizontal current with depth probably due to the complex bottom topography and the coastal configuration.

CONCLUDING REMARKS

Two-dimensional and three-dimensional hydrodynamical numerical model of the Yellow Sea and the East China Sea have been formulated to investigate tidal dynamics in the region.

Detailed comparison between the computed results and the available observations are provided. It was seen that there are good agreements between the model results and the observations for tidal elevations and tidal currents when the crudeness of tidal input data of open boundary along the continental shelf edge is considered.

Numerical experiments with the three-dimensional model to investigate the response of shelf sea to stationary uniform wind stress field have revealed that there are significant variation of magnitude and direction of horizontal current with depth.

Further refinement of the model is reserved until good quality of tidal data from the observation along the continental shelf edge are available.

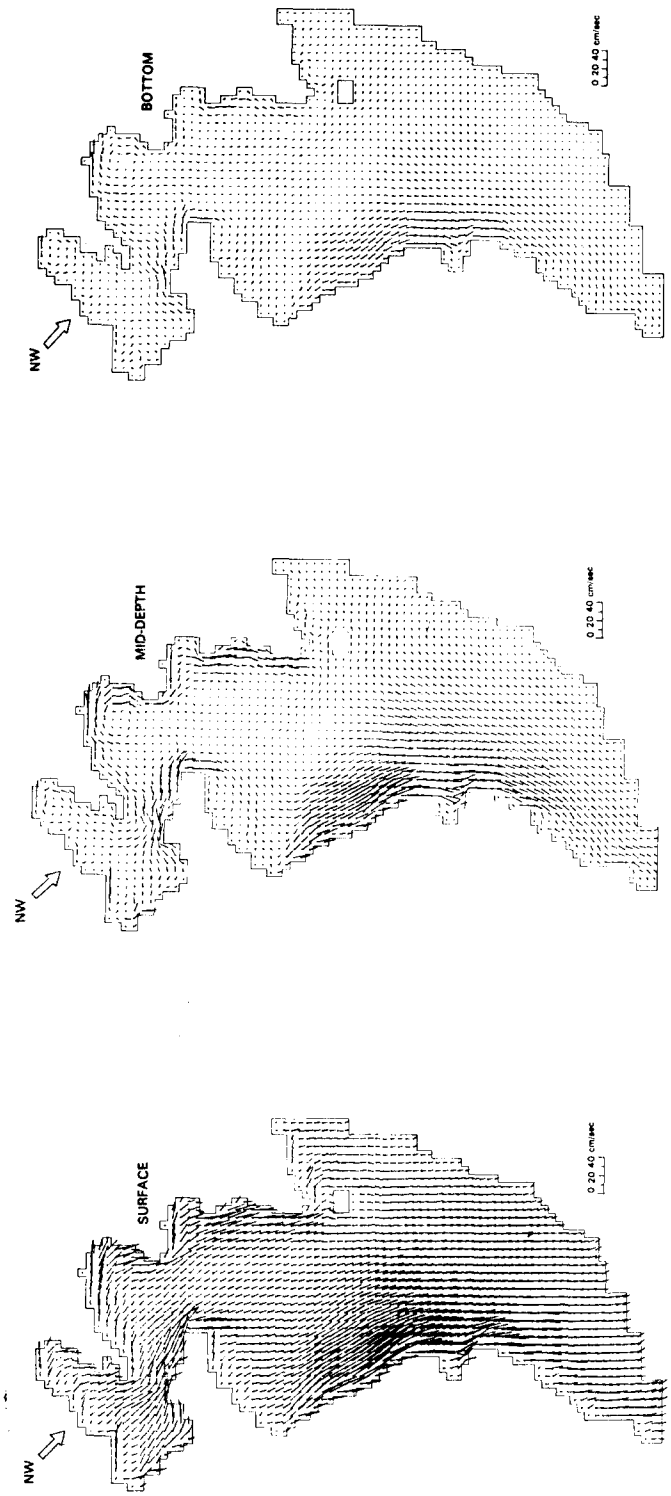

Fig. 18. The wind driven currents produced by a uniform northwesterly wind stress of 1.6dyn/cm^2.

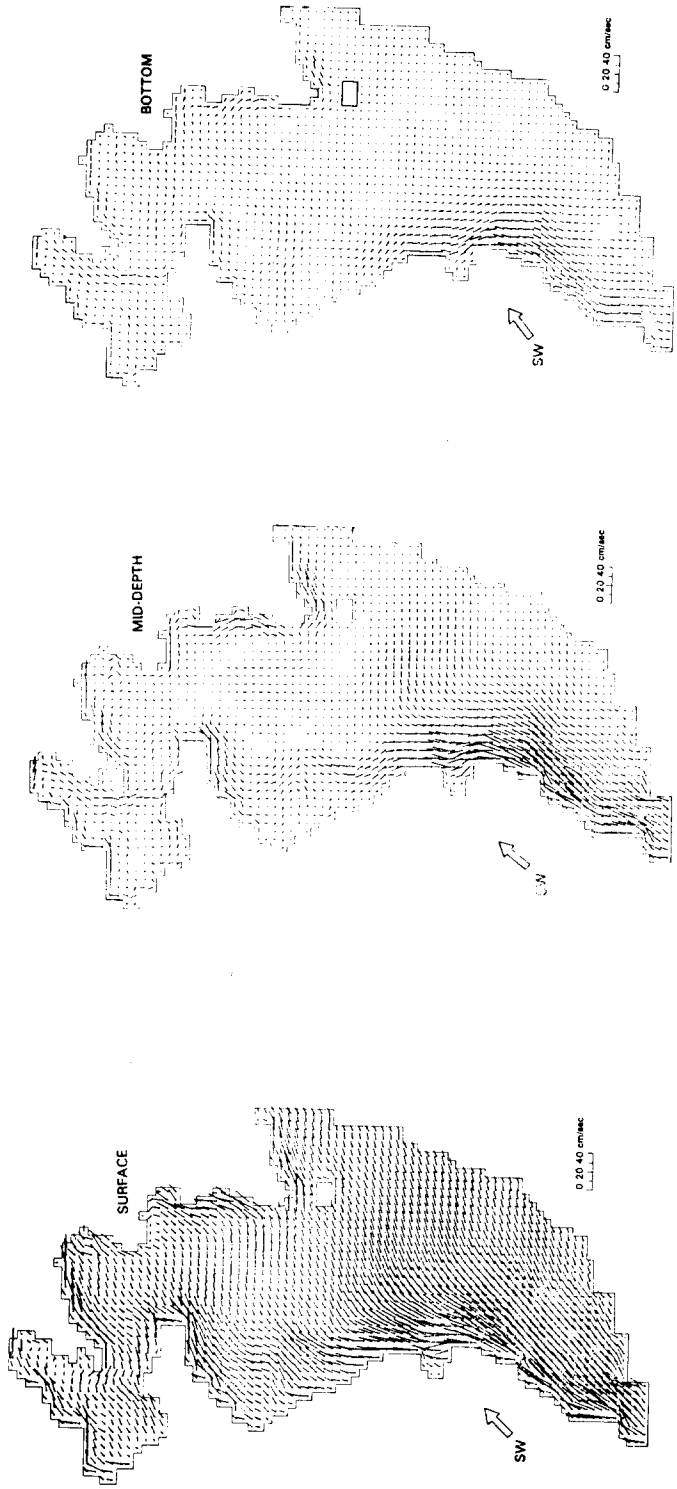

Fig. 19. The wind driven currents produced by a uniform southwesterly wind stress of 1.6 dyn/cm^2

ACKNOWLEDGEMENTS

Modelling work described here was initiated during my visit to I.O.S Bidston. The author is indebted to scientists in dynamic modelling group of Bidston Observatory. Funding for this work was provided by UNDP, British Overseas Development Administration and Korea Science and Engineering Foundation.

REFERENCES

Choi, B.H., 1980. A tidal model of the Yellow Sea and Eastern China Sea, Korea Ocean Research and Development Institute (KORDI), rep. 80-02, 72pp.

Davies, A.M., 1976. A numerical model of the North Sea and its use in choosing locations for the deployment of offshore tide gauges in the JONSDAP '76 oceanographic experiment, Deutsche Hydrographische Zeitschrift, 29 : 11-24.

Davies, A.M., 1980. On formulating a three-dimensional sea model with an arbitrary vertical eddy viscosity, Computer Methods in Applied Mechanics and Engineering, 22, 187-211.

Davies, A.M. and G.K. Furnes, 1980. Observed and computed M_2 tidal currents in the North Sea, Journal of physical Oceanography, 10, 237-257.

Defant, A., 1961. Physical Oceanography, 2 vols. Oxford, Pergamon Press. 729 and 598pp.

Flather, R.A. and N.S. Heaps, 1975. Tidal computations for Morecambe Bay, Geophysical Journal of the Royal Astronomical Society, 42 : 489-517.

Flather, R.A., 1976. A tidal model of the North-West European Continental shelf, Mémoires de la Société Royale des Sciences de Liège, ser. 6, 10 : 141-164.

Heaps, N.S., 1972. On the numerical solution of the three-dimensional hydrodynamical equations for tides and storm surges, Mém, Soc. Roy Sci. Liège, 2, 143-180.

Larsen, L.H. and G.A. Cannon, 1983. Tides in the East China Sea, Paper presented to Symposium on Sedimentation on the Continental Shelf, April 1983, Hangzhou, China.

Ogura, S., 1933. The tides in seas adjacent to Japan, Bulletin of Hydrographic Department, Imperial Japanese Navy, 7, 189pp.

Roberts, K.V. and N.O. Weiss, 1976. Convective difference schemes, Math. Comput. 20, 272-299.